Multi-Mode and Multi-Frequency Differential Lamb Wave Imaging with in situ Sparse Transducer Arrays

Jennifer E. MICHAELS and Thomas E. MICHAELS, School of Electrical and Computer Engineering, Georgia Institute of Technology, Atlanta, Georgia, USA

Abstract. Application of ultrasonic methods to structural health monitoring requires a compromise between coverage and complexity, making it desirable to use as few transducers as possible to cover the largest area. Such a consideration leads to the use of very sparse arrays where transducers are spatially distributed over a large area and are permanently attached to the structure. For plate-like geometries typical of many structural components, Lamb waves are the ultrasonic wave mode of choice because of their ability to propagate long distances while maintaining a reasonable signal-to-noise ratio. Lamb waves can be difficult to analyze due to both their dispersive nature and the presence of multiple modes. Here we consider both broadband and narrowband excitations of attached piezoelectric transducers, and propose analysis methods using signals recorded from all transducer transmit-receive combinations both before and after introduction of damage. Phased signal addition and image fusion algorithms that utilize information from multiple modes and frequencies are applied to the scattered signals, resulting in differential images of the structure. Results are presented for artificial defects in an aluminium plate, and are compared to those obtained using a single narrowband guided wave mode.

1. Introduction

Many applications utilizing guided waves for detecting damage rely upon narrowband signals containing one or two modes to minimize dispersion and facilitate interpretation. Pulse echo or through transmission echoes from specific modes may be detected and interpreted directly [1-3], or various beam forming algorithms can be used to generate images from transducer arrays [4-8]. Tomographic reconstruction methods have also been implemented to construct images from guided wave signals [9,10]. If only a single mode is present, dispersion compensation can be performed to map time to propagation distance and thus remove signal distortion [11]. Broadband signals containing multiple modes are more difficult to interpret, and various analysis schemes have been proposed to detect and localize damage based upon changes in waveforms [12,13].

In the work presented here, signals received before and after damage is introduced are filtered and differenced to obtain scattered signals from the damage. Differential images are generated from the scattered signals using a beam forming algorithm [5,14] in order to localize damage. Finally multiple images are fused, or combined together, to improve the signal-to-noise ratio and localization of damage. Results are shown for artificial damage in an aluminium plate.

2. Methodology

Consider a plate instrumented with a sparse array of N transducers located at known coordinates. If each transducer can act as either transmitter or receiver, then for a particular excitation, there are a total of $N!/[2(N-2)!]$ possible transmit-receive pairs. Depending upon the transducer design, it may be possible to excite separate Lamb wave modes by using different frequency excitations, or there could be multiple sparse arrays of sensors, with each array capable of exciting a different dominant mode. The goal is to acquire signals at different times, and to use changes in these signals to localize any damage that may have occurred in the interval between the acquisitions.

2.1 Signal Processing

Recorded signals could result from either a tone burst or broadband excitation. If a tone burst excitation is used, then the received signals are band limited and only those Lamb wave modes that could be generated by the transducer excitation are present. If a broadband excitation is used, such as is typically the case with a commercial spike mode pulser receiver, then the signal bandwidth is much larger and more modes will generally be present than for the tone burst excitation. It is then possible to apply a band pass filter to reduce the bandwidth and the number of modes. Thus, by either applying multiple tone burst excitations and acquiring multiple signals sets, or by applying multiple filters to a single set of broadband signals, it is possible to obtain sets of waveforms containing different mode and frequency information; the number of sets depends upon the number of arrays, excitations and filters.

For the work presented here, all signals were generated using a spike mode excitation. Subsequent filtering was accomplished by convolution with a three cycle tone burst at the desired frequency. For each frequency, the group velocity (c_g) was experimentally obtained from the six direct arrivals. The arrival time was determined by locating the first arrival of the envelope detected signal, and finding the cross time using a threshold equal to 25% of the peak amplitude. The group velocity was computed as the slope of the linear fit of distance vs. arrival time. The final signal processing step was to subtract baseline signals from those recorded after damage was introduced. These differenced signals contain information on energy scattered from any flaws and are used to generate images of damage.

2.2 Image Generation

Individual images are generated from a single set of differenced, or scattered, signals by creating an evenly spaced grid of points on the plate and considering each grid point to be a potential flaw. For each transducer transmit-receive pair, the arrival time of the signal scattered from a defect at the grid point is calculated assuming that there is no mode conversion and the group velocity is constant. A time window beginning at that arrival time is identified, and the windows from all signal pairs are summed. The energy of the summed signal becomes the image pixel value at that point. This process is repeated for every pixel of the image. In Equations (1), (2) and (3), (x_f, y_f) are the coordinates of the point on the image, (x_i, y_i) are the coordinates of the i^{th} transducer, t_{ij}^f *is* the time from the i^{th} transducer to the point (x_f, y_f) and then to the j^{th} transducer, $d_{ij}(t)$ is the signal recorded from transducer pair (i,j), $w(t)$ is a windowing function of width T, $s(t; x_f, y_f)$ is the summed signal over all transducer pairs, and $E(x_f, y_f)$ is the resulting image value at the point (x_f, y_f).

$$t_{ij}^{f} = \left[\sqrt{(x_i - x_f)^2 + (y_i - y_f)^2} + \sqrt{(x_j - x_f)^2 + (y_j - y_f)^2} \right] \Big/ c_g \quad (1)$$

$$s(t; x_f, y_f) = \sum_{i=1}^{N-1} \sum_{j=i+1}^{N} d_{ij}(t - t_{ij}^{f}) w(t - t_{ij}^{f}) \quad (2)$$

$$E(x_f, y_f) = \int_0^T s^2(t; x_f, y_f) dt \quad (3)$$

2.3 Image Fusion

Multiple images can be generated for the same plate condition by using each signal set to form an image. Image fusion refers to the combining, or fusing, of these images to obtain an improved image with perhaps better damage localization and signal-to-noise ratio.

The main objective of image fusion is to reduce artefacts that might be mistaken for damage. There are three primary categories of artefacts: (1) phasing artefacts where multiple peaks from the same echoes are alternately in phase and out of phase in a spatial neighbourhood, (2) extra signal artefacts caused by scattered echoes converted to other modes or reflected from geometrical features such as edges, and (3) signal alignment and distortion artefacts which occur when the two signals being subtracted do not perfectly match for reasons other than damage (e.g., temperature changes, surface variations, etc.). Since different frequencies and modes travel at different wave speeds and interact differently with flaws and geometry, these artefacts may appear at different locations on the various images, whereas it is expected that flaws would not. Thus it is reasonable to combine images to reduce the various artefacts.

Image fusion methods considered here are pixel-based, where the value of the pixel in the fused image is based only upon the corresponding pixels in all the component images; neighbouring pixels are not considered. One candidate fusion method is to simply take the minimum pixel value from all the images at each point. Other possible fusion methods include the arithmetic mean, the geometric mean, and the maximum. Since the goal is to reduce artefacts, the maximum is not appropriate. The risk in taking either the minimum or the geometric mean is that if a single image did not include the defect, then that defect would be missing in the fused image. Despite this risk, here we consider only the minimum, realizing that more sophisticated fusion algorithms would need to be considered prior to field implementation.

3. Experiments

A 6061 aluminium plate of dimensions 610 x 610 x 3.125 mm was instrumented with four piezoelectric transducers as summarized in Table 1. The transducers were fabricated at Georgia Tech from 12.5 mm diameter PZT disks backed with epoxy, and were attached to the plate using conductive epoxy. The transducers were driven and signals received using a commercial pulser receiver (Panametrics Model 5072PR) with spike mode excitation. Each measurement consisted of recording the set of signals from the six transducer pairs. Damage was introduced in the form of two through holes of 6 mm diameter; the locations are summarized in Table 1. Multiple signals were recorded from the undamaged plate and from the damaged plate after each hole was drilled. Signals were recorded under ambient conditions which were nominally identical; however, there were small temperature changes estimated to be less than ±2°C.

Table 1. Transducer and Hole Locations

Description	X Coordinate (mm)	Y Coordinate (mm)
Transducer #1	215.9	375.9
Transducer #2	398.8	419.1
Transducer #3	424.2	205.7
Transducer #4	180.3	221.0
Hole #1	355.6	329.4
Hole #2	279.4	152.4

Signals were filtered by convolution with 17 different 3-cycle tone bursts with frequencies of 140 kHz to 300 kHz at 10 kHz increments. Various signal pairs were directly subtracted after filtering, and all images were generated from the filtered, differenced signals. A variable width rectangular summing window was used with width inversely proportional to frequency, and was set to 3 μs at 200 kHz. For all frequencies considered, the S_0 Lamb wave mode was dominant, although signals contained evidence of smaller amplitude direct, mode-converted and reflected A_0 echoes.

4. Results

Figure 1 shows 220 kHz single images computed from signals recorded immediately before and after drilling of the two 6 mm diameter holes. The colour scale is normalized so that dark red corresponds to the peak intensity of the image and dark blue is zero.

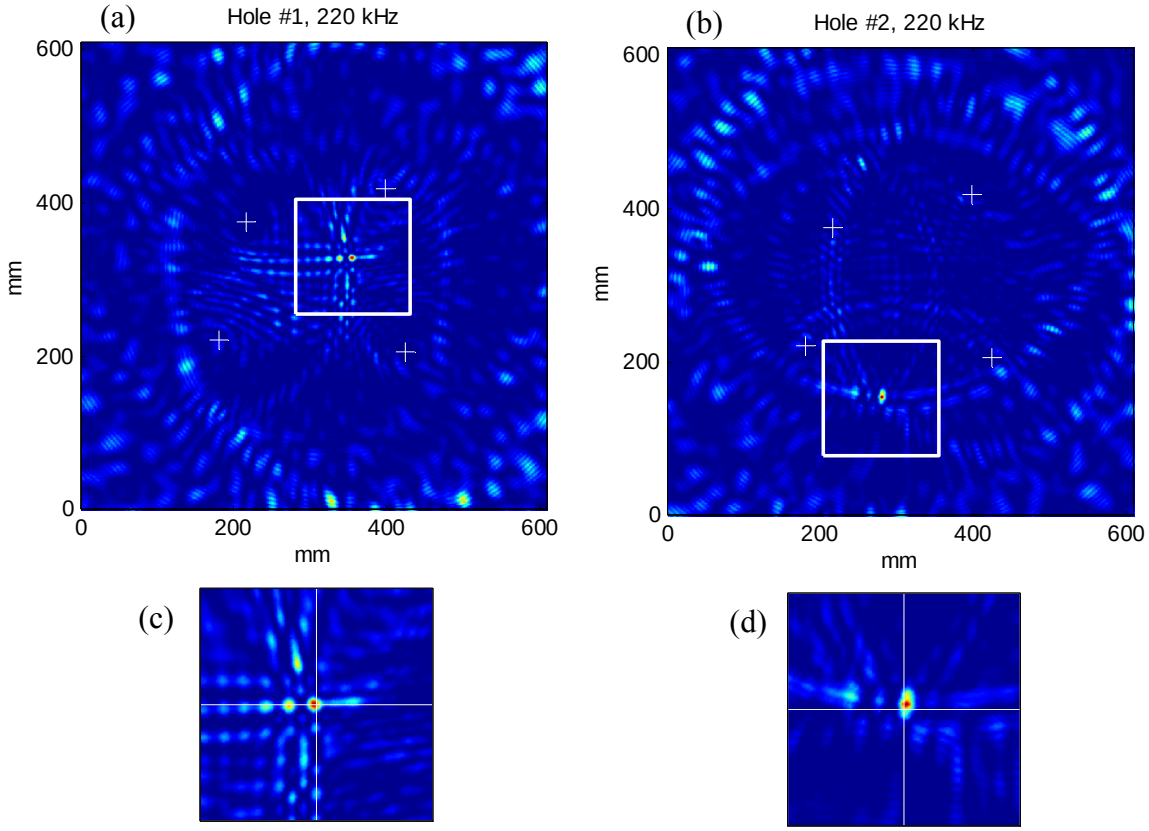

Figure 1. Sparse array images at 220 kHz. (a) Full image of hole #1, (b) full image of hole #2, (c), zoom of hole #1, and (d) zoom of hole #2. Boxes in the full images are zoomed areas. Transducer locations are denoted by the "+" symbol, and nominal flaw locations are indicated by the cross hairs in the zoomed images.

For both holes the flaw is imaged in the correct location (within experimental drilling error), and furthermore the strongest intensity pixel in the image is at the flaw, meaning that the flaw is unambiguously detected. However, there are clearly strong phasing artefacts, particularly for hole #1, as well as other artefacts caused by multiple reflections, mode conversion and alignment errors. Three figures of merit are defined for quantifying image quality: (1) location error, (2) image peak value away from the flaw, and (3) image standard deviation away from the flaw. The location error is the linear distance from the peak value point on the image to the nominal flaw location. A 50 mm diameter circle centred at the nominal flaw location is excluded from calculation of the peak value and standard deviation, and the image is normalized to a peak value of unity prior to these calculations. Results for the images of Figure 1 are shown in Table 2.

Table 2. Figures of Merit for the Single Images of Figure 1

Description	Location Error (mm)	Peak Value Away From Flaw	Standard Deviation Away From Flaw
Hole #1	2.63	0.752	0.0558
Hole #2	2.67	0.575	0.0539

The single images of Figure 1 can be compared to those obtained by fusing the multiple images obtained from the 17 frequency filters; these fused images are shown in Figure 2.

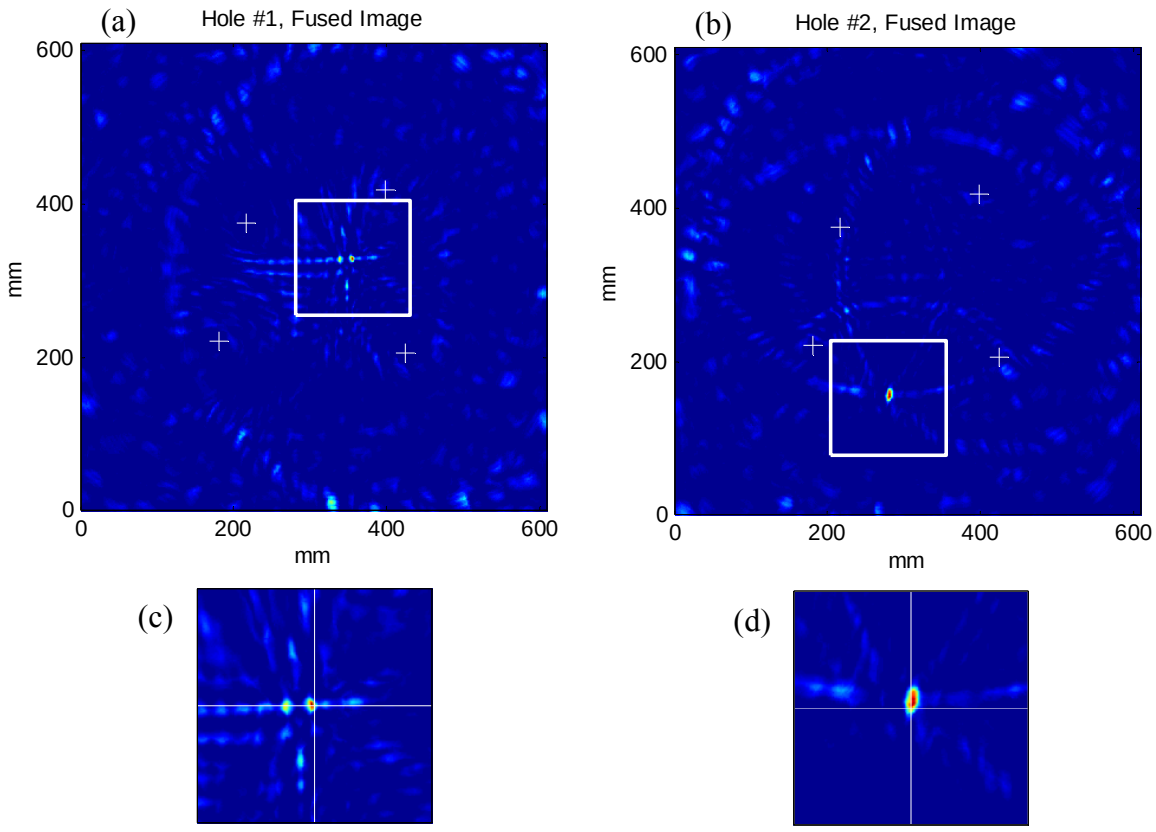

Figure 2. Fused images from 17 frequencies. (a) Full image of hole #1, (b) full image of hole #2, (c), zoom of hole #1, and (d) zoom of hole #2. Boxes in the full images are zoomed areas. Transducer locations are denoted by the "+" symbol, and nominal flaw locations are indicated by the cross hairs in the zoomed images.

Table 3 shows the corresponding figures of merit for the fused images, which can be compared to the single image values of Table 2.

Table 3. Figures of Merit for the Fused Images of Figure 2

Description	Location Error (mm)	Peak Value Away From Flaw	Standard Deviation Away From Flaw
Hole #1	1.71	0.571	0.0321
Hole #2	3.05	0.360	0.0298

The flaw locations have remained substantially the same, but both the peak value and standard deviation away from the flaw have decreased. Qualitatively the fused images are much "cleaner" and less cluttered than the individual images, although there are still noticeable artefacts.

The utility of image fusion is even more evident when considering the situation when the baseline signals are not well aligned with the flaw signals, such as is the case when there is a temperature change. Figure 3 shows sparse array images (single and fused) of hole #2 using a second baseline signal that was recorded at a slightly different temperature than the flaw signal; this unmeasured temperature difference was estimated to be less than 2ºC. Corresponding figures of merit are shown in Table 4.

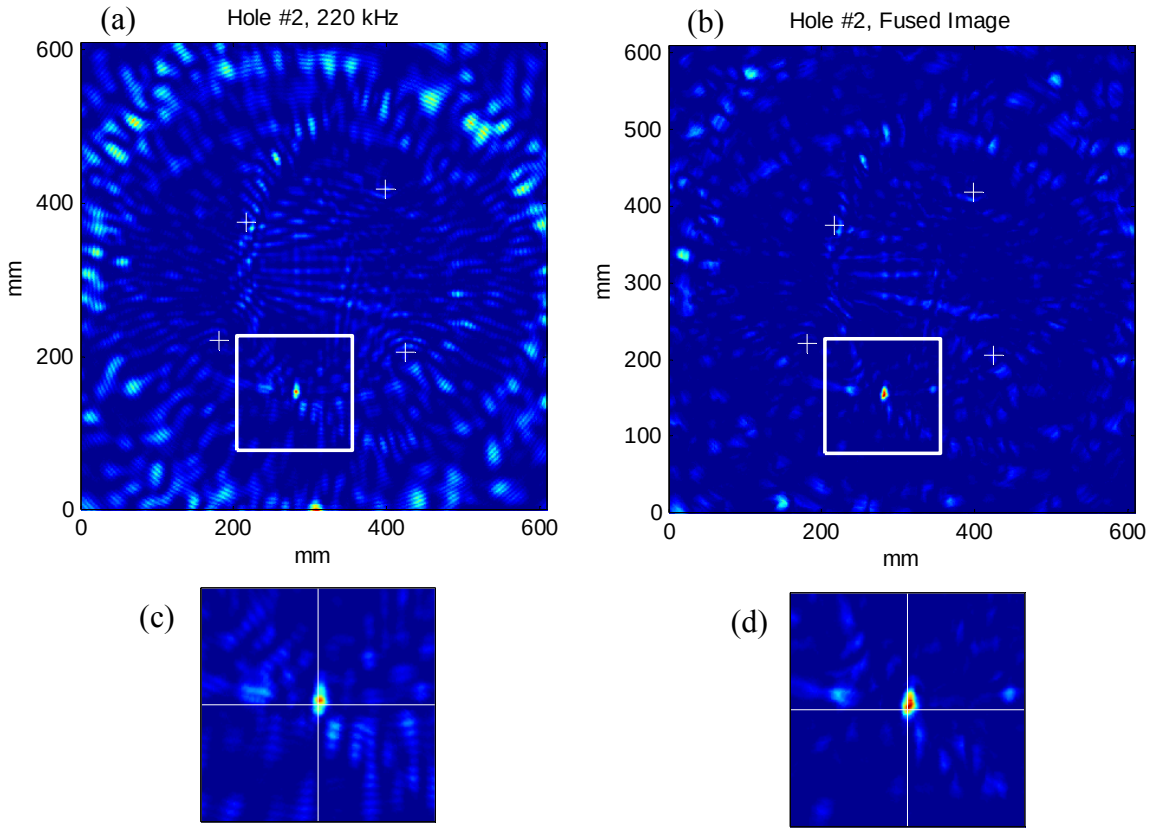

Figure 3. Sparse array images of hole #2 using a baseline signal that is not well-matched to the flaw signal. (a) Single image at 220 kHz, (b) fused image from 17 frequencies, (c), zoom of single image, and (d) zoom of fused image. Boxes in the full images are zoomed areas. Transducer locations are denoted by the "+" symbol, and nominal flaw locations are indicated by the cross hairs in the zoomed images.

Table 4. Figures of Merit for the Single and Fused Images of Figure 3

Description	Location Error (mm)	Peak Value Away From Flaw	Standard Deviation Away From Flaw
Hole #2, 220 kHz	153.72	1.000	0.0726
Hole #2, Fused	1.71	0.558	0.0379

The flaw can no longer be unambiguously detected from the single image since the largest intensity indications are from artefacts. The background standard deviation is also larger than from previous images. After image fusion the flaw is unambiguously detected and both the peak value and standard deviation are significantly reduced.

The effect of the image fusion process can best be seen by comparing individual and cumulative figures of merit as the fused image is formed. Figure 4 shows a plot of individual and cumulative peak value and standard deviation away from the flaw as each individual image is incorporated. The horizontal axis shows the frequency of the images in the order in which they are fused. The first image is the one in the centre of the bandwidth, 220 kHz, and subsequent images are fused by moving out from the centre frequency in an alternating pattern of lower and then higher frequencies until all 17 images are fused. For this particular case, the lower frequencies have lower intensity artefacts than the higher frequencies with the best individual performance at 160 kHz. The fused image has a slightly lower artefact intensity than that of the single image at 160 kHz but with a lower standard deviation, indicating that the fused image is less cluttered.

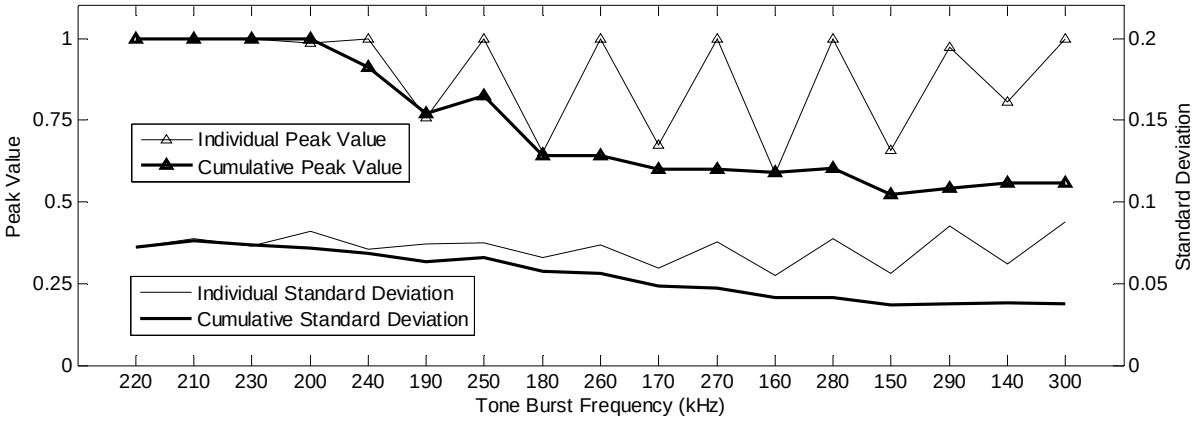

Figure 4. Individual and cumulative figures of merit for the fused image of Figure 3(b).

5. Discussion and Conclusions

In this paper a method of utilizing information from multiple modes and frequencies has been proposed for improving the quality of images constructed from sparse transducer arrays attached to plate-like structures. It has been demonstrated on a 3.175 mm thick aluminium plate from which broadband signals were obtained from glued-on piezoelectric disks. Results indicate that artefacts can be reduced and signal-to-noise ratio improved by fusing images obtained at different frequencies; it is anticipated that further improvement could be obtained by also including additional modes. For the experiments reported here, signals were dominated by the S_0 mode and there was insufficient energy in other modes to be able to utilize them.

There are several possible pitfalls that could occur by direct application of this methodology. The most serious one is that real flaws could be removed during the fusion process because of their absence from one or more of the images; improved fusion strategies should be employed to reduce the likelihood of this happening. Another potential problem is lack of registration between images. If there are errors in the frequency dependent group velocity, then the same flaw could be localized at different positions on the various frequency images, and thus be removed during the fusion process. This situation was not a problem for the results shown here, indicating that the experimental method for determining group velocity was effective. A third possible problem is uncorrected dispersion. For the frequencies and plate thickness considered here, dispersion was quite small and could be safely ignored. If significant dispersion is present, then phasing artefact patterns will change as a function of frequency, which could cause flaws to not overlap and thus be removed from the fused image. However, if dispersion curves are known, then dispersion compensation could be applied to avoid this problem [11]. Alternatively, images could be formed from envelope detected signals, which removes phasing artefacts at the expense of significant blurring [14]. Even though there are potential implementation challenges, the significance of this work is that it demonstrates the efficacy of systematically incorporating multiple guided wave modes and frequencies for improved detection and localization of damage.

References

[1] P. Cawley, M. J. S. Lowe, D. N. Alleyne, B. Pavlakovic, and P. Wilcox, "Practical Long Range Guided Wave Testing: Applications to Pipes and Rails," *Materials Evaluation*, **61**, pp. 66-74, 2003.

[2] P. S. Tua, S. T. Quek and W. Wang, "Detection of Cracks in Plates Using Piezo-Actuated Lamb Waves," *Smart Materials and Structures*, **13**, pp. 643-660, 2004.

[3] V. Giurgiutiu, "Tuned Lamb Wave Excitation and Detection with Piezoelectric Wafer Active Sensors for Structural Health Monitoring," *J. Intell. Mater. Syst. Struct.*, **16**, pp. 291-305, 2005.

[4] P. Wilcox, "Omni-Directional Guided Wave Transducer Arrays for the Rapid Inspection of Large Areas of Plate Structures," *IEEE Trans. Ultrason., Ferroelect., and Freq. Contr.*, **50**(6), pp. 699-709, 2003.

[5] C. H. Wang, J. T. Rose and F.-K. Chang, "A Synthetic Time-Reversal Imaging Method for Structural Health Monitoring," *Smart Materials and Structures*, **13**, pp. 415-423, 2004.

[6] V. Giurgiutiu and J. Bao, "Embedded-Ultrasonics Structural Radar for in situ Structural Health Monitoring of Thin-Wall Structures," *Structural Health Monitoring*, **3**(2), pp. 121-140, 2004.

[7] R. Sicard, A. Chahbaz and J. Goyette, "Guided Lamb Waves and L-SAFT Processing Technique for Enhanced Detection and Imaging of Corrosion Defects in Plates with Small Depth-to-Wavelength Ratios," *IEEE Trans. Ultrason., Ferroelect., and Freq. Contr.*, **51**(10), pp. 1287-1297, 2004.

[8] G. Konstantinidis, B. W. Drinkwater and P.D. Wilcox, "The Long Term Stability of Guided Wave Structural Health Monitoring Systems," *Review of Progress in Quantitative NDE*, **25B**, D. O. Thompson and D. E. Chimenti (Eds.), AIP, pp. 1702-1709, 2006.

[9] E. V. Malyarenko and M. K. Hinders, "Fan Beam and Double Crosshole Lamb Wave Tomography for Mapping Flaws in Aging Aircraft Structures," *J. Acoust. Soc. Amer.*, **108**(4), pp. 1631-1639, 2000.

[10] K. R. Leonard, E. V. Malyarenko and M. K. Hinders, "Ultrasonic Lamb Wave Tomography," *Inverse Problems*, **18**, pp. 1795-1808, 2002.

[11] P. D. Wilcox, "A Rapid Signal Processing Technique to Remove the Effect of Dispersion from Guided Wave Signals," *IEEE Trans. Ultrason., Ferroelect., and Freq. Contr.*, **50**(4), pp. 419-427, 2003.

[12] H. Gao, Y. Shi and J. L. Rose, "Guided Wave Tomography on an Aircraft Wing with Leave in Place Sensors," *Review of Progress in Quantitative NDE*, **24B**, D.O. Thompson and D.E. Chimenti (Eds.), AIP, pp. 1788-1794, 2005.

[13] C. Valle and J. W. Littles, "Flaw Localization Using the Reassigned Spectrogram on Laser-Generated and Detected Lamb Waves," Ultrasonics, **39**, pp. 535-542, 2002.

[14] J. E. Michaels and T. E. Michaels, "Enhanced Differential Methods for Guided Wave Phased Array Imaging Using Spatially Distributed Piezoelectric Transducers," *Review of Progress in Quantitative NDE*, **25A**, D.O. Thompson and D.E. Chimenti (Eds.), AIP, pp. 837-844, 2006.